

Signals of Statistical Anisotropy in WMAP Foreground-Cleaned Maps

Pramoda Kumar Samal¹, Rajib Saha², Pankaj Jain¹
John P. Ralston³

October 26, 2018

¹Department of Physics, Indian Institute of Technology, Kanpur, U.P,
208016, India

²Jet Propulsion Laboratory, M/S 169-327, 4800 Oak Grove Drive,
Pasadena, CA 91109; California Institute of Technology, Pasadena, CA
91125

³Department of Physics & Astronomy, University of Kansas, Lawrence, KS
66045, USA

emails: samal@iitk.ac.in, Rajib.Saha@jpl.nasa.gov, pkjain@iitk.ac.in, ralston@ku.edu

Abstract

Recently a symmetry-based method to test for statistical isotropy of the cosmic microwave background was developed. We apply the method to template-cleaned 3-year and 5-year WMAP-*DA* maps. We examine a wide range of angular multipoles from $2 < l < 300$. The analysis detects statistically significant signals of anisotropy inconsistent with an isotropic CMB in some of the foreground cleaned maps. We are unable to resolve whether the anomalies have a cosmological, local astrophysical or instrumental origin. Assuming the anisotropy arises due to residual foreground contamination, we estimate the residual foreground power in the maps. For the W band maps, we also find a highly improbable degree of isotropy we cannot explain. We speculate that excess isotropy may be caused by faulty modeling of detector noise.

1 Introduction

The inflationary Big Bang model assumes that anisotropies of the cosmic microwave background (*CMB*) come from random isotropic perturbations in the early universe. However there are indications that cosmological observables may not be isotropic. The indications include distributions of polarizations from radio galaxies (Birch 1982, Kendall and Young 1984, Jain and Ralston 1999, Jain and Sarala 2006), statistics of optical polarizations from quasars (Hutsemékers 1998, Hutsemékers and Lamy 2001, Jain *et al* 2004) and many studies of unpolarized *CMB* data. The *CMB* studies indicate an alignment of the low-*l* multipoles (de Oliveira-Costa *et al* 2004, Ralston and Jain 2004, Schwarz *et al* 2004) and a hemispherical anisotropy (Eriksen *et al* 2004). The indications of violation of isotropy in *CMB* data has prompted substantial activity with varying outcomes (Katz and Weeks 2004, Bielewicz *et al* 2004, Hansen *et al* 2004, Bielewicz *et al* 2005, Prunet *et al* 2005, Copi *et al* 2006, de Oliveira-Costa and Tegmark 2006, Wiaux *et al* 2006, Bernui *et al* 2006, Freeman *et al* 2006, Magueijo and Sorkin 2007, Bernui *et al* 2007, Copi *et al* 2007, Eriksen *et al* 2007b, Helling *et al* 2007, Land and Magueijo 2007, Pullen and Kamionkowski 2007, Lew 2008, Bernui 2008). Differences arise due to different tests being used by different authors (Efstathiou 2003, Hajian *et al* 2004, Hajian and Souradeep 2006, Donoghue and Donoghue 2005) and radio (Bietenholz and Kronberg 1984) data. Despite a measure of controversy, it is astonishing that diverse data sets all indicate a common

axis of anisotropy, pointing roughly in the direction of the Virgo supercluster (Ralston and Jain 2004).

The possible violation of statistical isotropy in CMB has lead to many theoretical studies (Cline *et al* 2003, Contaldi *et al* 2003, Kesden *et al* 2003, Berera *et al* 2004, Armendariz-Picon 2004, Moffat 2005, Gordon *et al* 2005, Land and Magueijo 2005, Vale 2005, Abramo *et al* 2006, Land and Magueijo 2006, Rakic *et al* 2006 Gumrukcuoglu *et al* 2006, Inoue and Silk 2006, Rodrigues 2008, Naselsky *et al* 2007, Campanelli *et al* 2007, Koivisto and Mota 2007, Boehmer and Mota 2008, Kahniashvili *et al* 2008, Dimopoulos *et al* 2008). The generation and evolution of primordial perturbations in an anisotropic universe has also been studied (Koivisto and Mota 2006, Battye and Moss 2006, Armendariz-Picon 2006, Pereira *et al* 2007, Gumrukcuoglu *et al* 2007) as well as the possibility of anisotropic inflation (Hunt and Sarkar 2004, Buniy *et al* 2006, Donoghue *et al* 2007, Yokoyama and Soda 2008, Kanno *et al* 2008, Erickcek *et al* 2008). The possibility that foreground contamination can lead to alignment has been investigated (Gaztanaga *et al* 2003, Slosar and Seljak 2004). Alternatively it has been suggested that systematic and statistical errors in the extracted CMB signal may lead to the observed anomalies (Liu and Li 2008). There have also been some theoretical studies of the optical alignment effect (Jain *et al* 2002, Payez *et al* 2008, Hutsemékers *et al* 2008). It may be possible to explain the violation of isotropy in CMB and radio polarizations due to some local effect. However the alignment of optical polarizations depends on redshift and hence cannot be attributed to a local effect (Jain *et al* 2002).

In a recent paper (Samal *et al* 2008) we introduced a new method for testing isotropy of *CMB* data. The method is based on identifying invariant relations between different multipoles. For each multipole $l \geq 2$ we identify three rotationally invariant eigenvalues of the *power matrix* A_{ij} , defined by

$$A_{ij} = \frac{1}{l(l+1)} \sum_{m,m'} a_{lm}^* (J_i J_j)_{mm'} a_{lm'} . \quad (1)$$

Here J_i ($i = 1, 2, 3$) are the angular momentum operators in representation l . The sum of the eigenvalues is the usual power C_l . The remaining independent combinations of eigenvalues provide information about the isotropy of the sample.

In an infinite isotropic sample all the eigenvalues of the power matrix would be equal. Statistical anisotropies in *CMB* data will certainly lead to

statistical fluctuations in the eigenvalues. We quantify the fluctuations by introducing the concept of *power entropy*. The eigenvectors of the matrix A_{ij} also contain additional information. Their orientation should be random in truly isotropic data. We define the “principal” eigenvector as the one associated with the largest eigenvalue. We then study the *alignment entropy*, which tests for alignment among different eigenvectors.

In Samal *et al* (2008), we studied the WMAP Interior Linear Combination (ILC) data set and restricted attention to the multipole region $l \leq 50$. In the present paper we study the individual foreground cleaned Differencing Assembly (DA) maps, $Q1$, $Q2$, $V1$, $V2$, $W1$, $W2$, $W3$, $W4$, also prepared by the WMAP team. We also extend the scope of analysis to the range $2 \leq l \leq 300$. As far as we know these are the first such tests for high multipoles. They illustrate the effectiveness of the method compared to others, such as Maxwell multipoles (Copi *et al* 2006, 2007, Weeks 2004, Katz and Weeks 2004), which run into combinatoric problems at high l (Dennis 2005). We do not use the ILC map, since it is not expected to be reliable for the large l range we consider here. At large l the WMAP team uses the bands $V1$, $V2$, $W1$, $W2$, $W3$, $W4$ for their final power extraction in the 3-year and 5-year analysis. The $Q1$ and $Q2$ bands were not used in WMAP power estimates since they were found to be significantly contaminated by foreground effects.

Our motivation for the study is twofold. First, we are interested in testing whether the anisotropies found in Samal *et al* (2008) continue to hold for a larger range of multipoles. Second, we wish to test whether additional anomalies in this data may exist. Our tests are not intended to determine whether anomalies come from some physical effect, contamination due to foregrounds, or correlations of noise.

In next Section we briefly review the methodology. In Section 3 we describe how the methodology is applied to the WMAP data. In Section 4 we give results for test of statistical isotropy using the power entropy. In Section 5 we test for alignment of different multipoles with the quadrupole axis. In Section 6 we test for statistical isotropy using the alignment entropy. We conclude in Section 7.

2 Covariant Frames and Statistics Across Multipoles

The *CMB* temperature fluctuation in each map is conventionally expanded in spherical harmonics

$$T(\hat{n}) = \sum_{lm} a_{lm} Y_{lm}(\hat{n}).$$

The usual power $C_l \sim \sum_m a_{lm} a_{lm}^*$ is rotationally invariant and has no information about anisotropy. The angular orientation of each mode is probed by a unique orthonormal frame $e_k^\alpha(l)$ and rotationally invariant eigenvalues $\Lambda_\alpha(l)$. These are obtained by diagonalizing the power tensor A , defined by

$$\begin{aligned} A_{ij} &= \langle a | J_i J_j | a \rangle, \\ &= \sum_{\alpha} e_i^\alpha (\Lambda^\alpha)^2 e_j^{\alpha*}. \end{aligned}$$

Here J_i is the rotation generator in representation l , and index l is suppressed when obvious.

Basic statistics derived from frames are the *power entropy* S_P and the *alignment entropy* S_X . Entropy is defined as in quantum statistical mechanics. The power density matrix $\rho_P = A/\text{tr}(A)$, where tr indicates the trace, is normalized, $\text{tr}(\rho_P) = 1$, to remove the power. The power entropy S_P for each multipole is

$$S_P = -\text{tr}(\rho_P \log(\rho_P)). \quad (2)$$

Isotropy predicts the maximum entropy

$$S_P \rightarrow \log(3) \quad (\text{isotropy}).$$

Small values of S_P indicates anisotropy. Note these measures apply mode-by-mode. The full range is $0 \leq S_P \leq \log(3)$, where $S_P \rightarrow 0$ for a “pure state” $\tilde{\Lambda}_1 = 1$ aligned along a single axis.

The alignment entropy S_X is a measure of alignment of frame axes. Let $e^i(l)$ be the “principal eigenvector” of the power tensor, meaning the one with the largest eigenvalue. Construct a 3×3 matrix X_{ij} :

$$X_{ij} = \sum_{l=l_{min}}^{l_{max}} e^i(l) e^j(l). \quad (3)$$

This tensor probe effectively averages over a range of multipole moments. Normalize by computing $\tilde{X} = X/\text{tr}(X)$. The alignment entropy is

$$S_X = -\text{tr}(\tilde{X} \log \tilde{X}).$$

3 Application to WMAP data

We use the WMAP 3-year and 5-year data for our analysis. The WMAP team (Hinshaw *et al* 2003, 2007) provides foreground-cleaned maps for the Q, V and W bands. The V and W bands are used for power spectrum estimation. The Q band is not used since it is found to be significantly foreground contaminated. The foreground removal method adopted by WMAP is incomplete in the galactic plane. This region is removed by using the *Kp2* mask before power spectrum estimation. Applying *Kp2* mask also eliminates emissions from the resolved point sources by removing circular area of radii 0.6° around the position of each of the sources. There also exist other foreground cleaning procedures that may be interesting to compare (Tegmark *et al* 2003, Saha *et al* 2006, Eriksen *et al* 2007a). Here we study only the foreground cleaned maps provided by the WMAP team.

3.1 Data Preparation

We apply the *Kp2* mask to all the individual foreground cleaned DA maps. The masked region is filled by a randomly generated CMB signal along with simulated detector noise based on WMAP's noise characteristics appropriate to each of the 8 maps.

Noise maps are generated as follows. Let σ_0 be the noise per observation of the detector under consideration. Let N_{pix} denote the number of pixels in each $N_{side} = 512$ level resolution map, and N_p be the effective number of observations at each pixel. Sample a Gaussian distribution with zero mean and unit variance N_{pix} number of times. Multiply each Gaussian variable by $\sigma_0/\sqrt{N_p}$ to form realistic detector noise maps.

Graphics of the 8 maps used in our study are shown in Fig. 1. There is no visible signature of galactic foreground contamination in the maps. Detector noise is evident in the W band DA maps.

3.2 Null Distributions

Statistical baselines were developed from 10,000-run simulations of isotropic random *CMB* power normalized to the data maps and including detector noise appropriate to each band. We set *preliminary* levels of statistical significance using *P*-values of 0.05 or less. *P* values are defined by the relative frequency for a statistic to occur with *P* or less. The significance level of collections of *P*-values is estimated using the binomial distribution of “pass” and “fail” outcomes. The probability to encounter *k* instances of passing defined by probability *p* in *n* trials is

$$P_{bin}(k, p, n) = p^k(1 - p)^{(n-k)}n!/(n - k)!k!.$$

The binomial distribution is well-known, and we also verified the distribution describes *P* values from the null simulations. In assessing many *P*-values we report the cumulative binomial probabilities

$$P_{bin}(k \geq k_*, p, n) = \sum_{k=k_*}^n P_{bin}(k, p, n).$$

4 Power Entropy

Fig. 2 shows the null distribution of power entropy for the *Q1* map over the multipole range $2 \leq l \leq 300$. The distributions of all the maps remains the same whether or not detector noise is added to the simulation.

Fig. 3 shows *P* values obtained from the WMAP data for the entire range, $2 \leq l \leq 300$, of multipole values considered. The horizontal dashed line indicates *P* = 0.05. Violation of statistical isotropy is indicated for many multipoles in all the bands. Table 1 (2) lists the 3-year (5-year) multipoles for different bands with *P*-values potentially inconsistent with isotropy.

Fig. 4 illustrates the entropy distributions leading to these *P*-values. A contour for the 95% confidence level is shown in gray. The 90% and 50% confidence level contours are also shown as curves. The relatively large spread of the distribution towards the small-*l* region is kinematic, akin to cosmic variance. The statistically anisotropic multipoles shown by red points are the same as those shown in Table 1.

<i>Band</i>	<i>Multipoles</i>
Q1	14, 17, 41, 52, 63, 94, 118, 128, 165, 178, 180, 185, 204, 206, 216, 222, 224, 231, 243, 246, 261, 279, 280, 282, 283, 287, 290, 294, 299
Q2	13, 14, 17, 41, 52, 54, 63, 94, 128, 180, 191, 204, 206, 227, 228, 246, 251, 261, 287, 289, 290, 294
V1	13, 14, 17, 41, 51, 52, 98, 118, 128, 165, 180, 191, 204, 206, 208, 218, 222, 227, 252, 261
V2	14, 17, 30, 41, 52, 64, 128, 180, 191, 201, 203, 218, 228
W1	13, 14, 17, 30, 41, 52, 120, 180, 185, 201, 208, 209, 218, 224, 231, 267, 269
W2	14, 17, 30, 40, 41, 52, 64, 98, 128, 155, 165, 178, 180, 210, 248, 261
W3	14, 17, 30, 41, 52, 54, 94, 101, 149, 180, 218, 222, 252, 286, 299
W4	13, 14, 51, 52, 64, 128, 135, 178, 189, 203, 206, 209, 218, 275, 291

Table 1: List of multipoles with $P < 0.05$ for power entropy for the 3-year WMAP-DA maps.

<i>Band</i>	<i>Multipoles</i>
Q1	14, 17, 41, 52, 94, 128, 135, 165, 177, 178, 180, 185, 191, 204, 206, 216, 218, 221, 222, 225, 231, 261, 290, 294
Q2	13, 14, 17, 41, 52, 54, 94, 128, 165, 170, 180, 191, 204, 206, 228, 246, 251, 261, 290, 294
V1	13, 14, 17, 41, 52, 54, 64, 101, 128, 165, 180, 191, 204, 206, 218, 222, 231, 252, 290
V2	14, 17, 30, 41, 52, 64, 94, 128, 161, 165, 180, 201, 204, 209, 218, 228
W1	13, 14, 17, 30, 41, 52, 64, 120, 128, 139, 180, 185, 201, 204, 210, 218, 224, 228, 231, 269
W2	13, 14, 30, 40, 41, 52, 98, 115, 128, 155, 165, 178, 180, 210, 231, 241, 246, 258, 261
W3	13, 14, 17, 41, 52, 54, 94, 101, 160, 180, 185, 228, 246, 249
W4	13, 14, 41, 52, 64, 94, 128, 135, 170, 180, 189, 201, 204, 206, 210, 241, 242, 252

Table 2: List of multipoles with $P < 0.05$ for power entropy for the 5-year WMAP-DA maps.

4.1 Significance: Power Entropy Statistics

We now assess the significance of the numerous small P -values observed for the power entropy.

Table 1 (2) shows 29 (24), 22 (20), 20 (19), 13 (16), 17 (20), 16 (19), 15 (14) and 15 (18) power entropies with P -value ≤ 0.05 for the 3-year (5-year) $Q1$, $Q2$, $V1$, $V2$, $W1$, $W2$, $W3$ and $W4$ maps respectively. The threshold values (upper bounds of P -values) for these power entropies estimated using the individual maps are given by $\mathcal{P} = 0.048$ (0.047), 0.0467 (0.049), 0.049 (0.049), 0.0412 (0.048), 0.0438 (0.049), 0.0483 (0.047), 0.0472 (0.047), 0.0473 (0.049). The total number of independent trials for $2 \leq l \leq 300$ is $n = 299$. From the binomial distribution the *cumulative* probabilities of obtaining $P_{bin}(k \geq k_{data}, P_{data}, 299)$ are shown in Table 3 for the eight maps from $Q1$ to $W4$ for the 3-year and 5-year data.

Clear violation of statistical isotropy is observed for $Q1$ and $Q2$ maps for both the 3 and 5-year data. which all have $P < 0.05$. We noticed in our study that the $Q1$ and $Q2$ P -values are correlated over all l , so we cannot consider them independent. Nevertheless the cumulative probability of 3×10^{-4} for the $Q1$ band is far below anything expected from an isotropic ensemble.

If one assumes each probability is independent - which is certainly an idealization - the binomial probability for $Q1$ and $Q2$ for the 3 year data to have such small probabilities is about 1.6×10^{-2} . Fig. 5 shows the probability of these outcomes over all bands as the “pass-value” $P_{band} < P_*$ is adjusted for both the 3 and 5 year data. The small P_{net} values show violation of isotropy. The entire data over all bands shows violation of isotropy with a binomial probability of 2.0×10^{-3} and 7.2×10^{-3} for the 3 and 5 year data respectively.

Since the 5 % P -val cut is somewhat arbitrary, Fig. 6 shows the cumulative probability of these outcomes over the $Q1$ and $Q2$ DAs as the “pass-value” $P_{band} < P_*$ is adjusted for both the 3 and 5-year data. The small P_{net} values show violation of isotropy. The cumulative probability for the remaining six DAs is shown in Fig. 7. Here we notice that the 3-year data does not show a significant violation of isotropy. However the signal of anisotropy is stronger in the 5 year data. The trend in this figure suggests that we may expect a much stronger signal of anisotropy in V and W bands as more data is accumulated.

Band	$Q1$	$Q2$	$V1$	$V2$
Significance (3 year)	3×10^{-04}	2.5×10^{-02}	0.10	0.46
Significance (5 year)	8.2×10^{-03}	0.10	0.15	0.36
Band	$W1$	$W2$	$W3$	$W4$
Significance (3 year)	0.17	0.37	0.44	0.44
Significance (5 year)	0.10	0.11	0.54	0.22

Table 3: Net significance of observing $P \leq 0.05$ -values shown in Table 1 (3 year) and Table 2 (5 year).

5 Alignment with the Quadrupole

Many authors (de Oliveira-Costa *et al* 2004, Ralston and Jain 2004, Schwarz *et al* 2004) have observed a strong alignment between the CMB quadrupole and the octopole. The power of both quadrupole and octopole appears to approximately lie in a plane. The perpendicular to the plane points roughly in the direction of the Virgo supercluster for both these multipoles. It has also been noted that these axes align closely with the CMB dipole, as well as with independent cosmological observations. Statistically significant alignment of several independent axes violates the hypothesis of statistical isotropy. As reported earlier, the WMAP-ILC map shows statistically significant signals of alignment with the quadrupole axis in the low l multipole range $l \leq 50$.

In our formalism one may construct an unbiased measure of alignment between multipoles by comparing the principal eigenvectors of the power tensor. In isotropic data these eigenvectors would point in random directions. The probability for isotropically distributed axes \hat{n} and \hat{n}' to align within θ is given by

$$P(\cos \theta) = (1 - \cos \theta) \quad (4)$$

where $\cos \theta = |\hat{n} \cdot \hat{n}'|$.

5.1 Significance of Axial Alignments

Table 4 (5) lists the multipoles with $P(\cos \theta) < 0.05$ for alignment with the quadrupole for 3-year (5-year) WMAP maps. There are 13 (12), 9 (12), 14 (15), 18 (17), 13 (20), 13 (15), 12 (12) and 11 (18) axes which show alignment with the quadrupole moments for the $Q1$, $Q2$, $V1$, $V2$, $W1$, $W2$, $W3$ and $W4$ maps respectively for 3-year (5-year) data. The threshold values (upper bound of the P values) are given by $\mathcal{P} = 0.046$ (0.041), 0.049 (0.047), 0.038

$Q1$	$Q2$	$V1$	$V2$	$W1$	$W2$	$W3$	$W4$
2	2	2	2	2	2	2	2
28	28	40	28	28	10	28	40
61	61	50	61	61	28	61	61
63	88	61	63	63	61	62	63
75	101	66	66	81	63	63	88
88	145	75	75	88	75	66	102
105	172	88	81	101	88	75	129
129	176	174	88	133	110	88	133
134	187	198	129	172	129	129	139
140	212	207	144	174	182	133	140
144		226	172	176	197	177	243
145		270	174	182	235	179	272
172		278	182	267	267	265	
182		289	187	279	270		
		293	207				
			243				
			267				
			279				
			293				

Table 4: List of multipoles with $P < 0.05$ for alignment with the quadrupole for 3-year WMAP data for all the maps for the multipole range $2 \leq l \leq 300$.

$Q1$	$Q2$	$V1$	$V2$	$W1$	$W2$	$W3$	$W4$
2	2	2	2	2	2	2	2
40	40	40	28	28	28	40	3
42	42	42	40	40	40	50	40
61	61	50	50	61	50	61	42
75	88	61	61	63	61	75	61
81	101	75	63	75	63	88	63
88	134	88	66	81	75	133	88
101	172	101	75	88	88	226	101
105	176	129	88	101	133	236	129
129	187	140	101	129	179	243	133
134	195	174	129	133	182	265	139
182	238	182	172	172	207	270	172
		207	174	174	267		176
		279	182	178	270		177
		300	187	182	171		197
			279	187			243
			293	234			266
				267			272
				278			
				279			

Table 5: List of multipoles with $P < 0.05$ for alignment with the quadrupole for 5-year WMAP data over the multipole range $2 \leq l \leq 300$.

(0.046), 0.048 (0.05), 0.048 (0.049), 0.048 (0.049), 0.044 (0.05), 0.049 (0.049). The binomial probabilities for each band are respectively 0.62 (0.57), 0.96 (0.74), 0.25 (0.39), 0.19 (0.31), 0.68 (0.091), 0.68 (0.50), 0.66 (0.82), 0.87 (0.22) for the 3-year (5-year) data. Including the effects of the search over $2 < l \leq 300$, the set of multipole axes examined shows no statistically significant signal of alignment. We point out, however, that the overall probabilities have a tendency to decrease as we go from three to five year data.

There are several differences between the data set used in the previous study and the one used for the present analysis. The previous study used the ILC map, which is ideal for low l multipoles. This is because the ILC map has lower foregrounds and the entire map can be used. The template cleaned maps are best suited for large l multipoles and require a mask to remove the contamination due to galactic and point source emissions. In addition, the high l data also contains very large detector noise contamination, tending to decrease signal-to-noise.

6 Alignment Entropy

We next consider the alignment entropy S_X over the entire range of multipoles $2 \leq l \leq 300$, and a few selected subsets, $150 \leq l \leq 300$ and $250 \leq l \leq 300$. Figs. 8 and 9 show null distributions of S_X for the range $150 \leq l \leq 300$ and $2 \leq l \leq 300$. These distributions are generated by simulated CMB data along with detector noise, appropriate for a particular map. The distributions of S_X for the two cases are nearly identical. These distributions are similar to the power entropy distributions, consisting of sharp suppression of small S_X below a peak near the maximum. The S_X distributions for small l show a long tail. Figs. 8 and 9 also show the value of S_X obtained from the data for all cases except the maps $Q1$ and $Q2$. For these two maps the value of S_X lies outside the range shown in the plots.

The values of S_X for all the maps for the three year WMAP data are shown in Table 6. The probabilities of obtaining these values from a random isotropic sample are also shown. These are computed by using 10,000 randomly generated samples of isotropic *CMB* maps including detector noise. The statistics are interesting. In all three sets the Q band shows a very significant signal of violation of statistical isotropy. The probability that the entropy obtained for $Q1$ map arises by a random fluctuation is less than 0.01 % for all three range of multipoles considered. The map $Q2$ also shows very

low probability values.

The preferred axes of alignment over the different ranges of multipoles are given in Table 7. We find that the axes do not point towards any familiar direction. The axes do not point towards Virgo and hence are not aligned with the quadrupole. They tend to lie within about 30° from the galactic plane at the galactic longitude ranging between 90° to about 100° . We next determine the mean axis in a simulated $Q1$ map in the range $2 \leq l \leq 300$. Foregrounds are added to this map by using the publicly available Planck Sky Model (PSM) ¹ as reference templates. We add foregrounds at the level of 1%, 2%, ..., 10% of the total contamination and determine the mean vector for each map. The mean vector is determined after applying the Kp2 mask and filling the masked region with randomly generated data, exactly as done for the real data set. As expected at low foreground level the mean axis fluctuates considerably for different realizations of the randomly generated maps. However at foreground levels of 5 % or higher, the mean axes stabilize. They also do not show much change with the increase in the level of contamination. The axes are found to lie between $b = 25^\circ - 28^\circ$, $l = 150^\circ - 167^\circ$ for foreground levels of 5 % or higher of their total values.

We compare the axes obtained using randomly generated maps with the axes given in Table 7. We find that the galactic latitude matches well with that obtained from the real data. However the longitude is off by almost $60^\circ - 70^\circ$. Hence it is not possible to assign the alignment we find to contamination due to known foregrounds. The randomly generated axes depend to some extent on the range of multipoles studied. For the multipole range $250 \leq l \leq 300$, the mean axis is found to be roughly $b = 6^\circ$, $l = 125^\circ$. This is a little closer to corresponding value in this range in Table 7. We notice, however, that dependence of the axis on the choice of multipole range is much stronger in the randomly generated data in comparison to that found in Table 7. This again shows that we cannot attribute the anisotropy in Q band to known foregrounds. It is possible that the anisotropy arises due to an unknown foreground source or from a combination of foregrounds and other effects.

The V and W bands reveal an unexpected number of cases with very *large* alignment entropy, corresponding to unusually *perfect* isotropy. We find several cases in the W band where the alignment entropy is so large

¹We acknowledge the use of version 1.1 of the Planck reference sky model, prepared by the members of Working Group 2 and available at www.planck.fr/heading79.html.

	Q1	Q2	V1	V2	W1	W2	W3	W4
$S_X(150, 300)$	0.98522	1.02024	1.09499	1.08822	1.09174	1.09234	1.08222	1.05858
$P(\%)$	<0.01	<0.01	99.25	72.08	99.98	>99.99	>99.99	82.10
$S_X(250, 300)$	0.79763	0.92503	1.077021	1.08415	1.055178	1.07635	0.98258	1.019228
$P(\%)$	<0.01	0.36	94.72	94.89	97.36	99.9	86.56	92.03
$S_X(2, 300)$	1.0636	1.0745	1.0964	1.0932	1.0967	1.0937	1.0920	1.0818
$P(\%)$	<0.01	0.15	95.86	53.94	99.94	99.74	99.91	65.52

Table 6: Alignment entropy S_X and corresponding P values (in %) for WMAP 3-year maps over the three multipole ranges, $2 \leq l \leq 300$, $150 \leq l \leq 300$ and $250 \leq l \leq 300$.

Q1 band	b (deg)	l (deg)
$150 \leq l \leq 300$	27.8	97.8
$250 \leq l \leq 300$	30.2	101.5
$2 \leq l \leq 300$	24.7	92.9
Q2 band	b (deg)	l (deg)
$150 \leq l \leq 300$	26.3	94.6
$250 \leq l \leq 300$	28.1	99.2
$2 \leq l \leq 300$	22.2	89.7

Table 7: The galactic latitude (b) and longitude (l) for the principal axis for the specified range of multipole moments for WMAP 3-year Q1 and Q2 bands

that the probability to obtain this from a random sample exceeds 99.99 %.

Similar results are seen for the five year WMAP data. In Table 8 we show the alignment entropy S_X and probabilities P for all the maps in the three multipole ranges considered. We again find that the Q band shows a very striking signal of anisotropy. The W band, on the other hand, again shows an improbably high level of isotropy. The V band does not appear statistically unusual. Table 9 shows the axes of alignment for the Q band. The axes are found to be consistent with that found in the three year data.

Fig. 10 shows the net probability across bands for $P < P_*$ or “excessive anisotropy” as well as $P > P_*$, or “excessive isotropy” for the 5 year data.

6.1 Foreground contamination in Q band

One might naturally assume the anisotropy found in the Q band would be due to foreground contamination. The principal vectors for all the mul-

	Q1	Q2	V1	V2	W1	W2	W3	W4
$S_X(150, 300)$	1.00795	1.02283	1.09116	1.08587	1.08633	1.09417	1.09522	1.08451
$P(\%)$	<0.01	<0.01	75.7	31.5	87.8	>99.99	>99.99	94.3
$S_X(250, 300)$	0.85946	0.89287	1.08185	1.08579	1.08321	1.08854	1.05246	1.07737
$P(\%)$	<0.01	<0.01	86.0	85.9	98.8	99.9	96.9	99.4
$S_X(2, 300)$	1.07100	1.07602	1.09462	1.09283	1.09362	1.09259	1.09694	1.08896
$P(\%)$	<0.01	<0.01	60.1	28.6	83.3	93.6	99.98	61.6

Table 8: The alignment entropy and the corresponding P values (in %) for the WMAP 5-year DA maps. The results for all the three multipole ranges considered in this paper are shown.

Q1 band	b (deg)	l (deg)
$150 \leq l \leq 300$	24.6	98.2
$250 \leq l \leq 300$	27.3	103.2
$2 \leq l \leq 300$	20.2	93.1
Q2 band	b (deg)	l (deg)
$150 \leq l \leq 300$	29.6	94.7
$250 \leq l \leq 300$	32.2	97.3
$2 \leq l \leq 300$	24.0	88.9

Table 9: The galactic latitude (b) and longitude (l) for the principal axis for the specified range of multipole moments for WMAP 5-year Q1 and Q2 bands

maps	Q1	Q2
Average		
Foreground	420.72 (3-year)	330.48 (3-year)
Power (μK^2)	417.33 (5-year)	375.73 (5-year)

Table 10: The average foreground residual power, $\langle l(l+1)C_l^{fg} \rangle / (2\pi)$, for the WMAP 3-year and 5-year Q1 and Q2 maps, which show significant signals of anisotropy with $P \leq 0.01$ % for the multipole range $150 \leq l \leq 300$. The foreground power has been averaged over this range of multipoles, as explained in text.

tipole ranges considered here cannot be consistently attributed to known foregrounds. Let us nevertheless assume that foregrounds give a significant contribution to the Q band anisotropy, and seek the mean foreground power required to explain the observations. We restrict this study to the multipole range $150 \leq l \leq 300$.

To estimate residual foreground contamination in the maps we use PSM as reference templates. We first generate a composite foreground map corresponding to each map using synchrotron, dust and free-free maps obtained by PSM. We apply the $Kp2$ mask to all the composite foreground maps also in order to avoid strong contamination arising from the galactic region. Finally we add a small fraction of the composite foreground contamination arising from these masked templates to a randomly generated CMB map, plus simulated detector noise appropriate to each maps. We finally compute the alignment entropy for each band.

The residual foreground contamination in regions not affected by the $Kp2$ mask was estimated from the fraction of the composite masked foreground template added to randomly generated CMB maps. We obtain the full-sky estimates of the foreground contamination using the MASTER method (Hivon *et al* 2002) which employs inversion of the mode-mode coupling matrix to convert the partial-sky power spectrum to full-sky estimates.

In Fig. 11 we show the alignment entropy as a function of the average value of the full-sky estimates of the residual foreground contamination for each band for the multipole range $150 \leq l \leq 300$. We estimate the average foreground power for the range of multipole moment $l_{min} \leq l \leq l_{max}$ as,

$$\langle l(l+1)C_l^{fg} \rangle = \frac{1}{(l_{max} - l_{min} + 1)} \sum_{l=l_{min}}^{l_{max}} l(l+1)C_l^{fg}, \quad (5)$$

where C_l^{fg} is the foreground power spectrum at l . For a given value of the

entropy obtained from the data this figure gives the average level of residual foreground contamination in the range of multipoles under consideration. The $Q1$ and $Q2$ maps indicate a strong level of foreground contamination for the multipole range $150 \leq l \leq 300$. Table 10 shows the estimated residual foreground contamination quantitatively.

6.2 Isotropy in V and W bands

The very striking result seen in Table 6 is the unusually high P-values for many of the multipoles in the V and W bands for the three year WMAP data. This anomaly is also supported by the WMAP five year data for the W band. This is very unexpected and shows a statistically unusual high level of isotropy. We are unable to identify the cause of this anomaly. One possibility is the neglect of noise correlations in our analysis. The anomaly is ameliorated if we artificially lower the detector noise level in the simulated random maps. The σ_0 values used for generating the noise maps for the bands $Q1$, $Q2$, $V1$, $V2$, $W1$, $W2$, $W3$, $W4$ are 2.245, 2.135, 3.304, 2.946, 5.883, 6.532, 6.885, 6.744, respectively. Fig. 12 shows the generated noise maps for the bands $Q1$ and $W2$. The $W2$ map over the range $150 \leq l \leq 300$ shows a P -value of 100%. To explore this, we studied how the P-value changes using a smaller value of σ_0 . Reducing σ_0 by two units to 4.532, the P-value decreases to a more reasonable value of 92%. However we find such a large change in the value of σ_0 unacceptable. The problem of statistically unlikely isotropy is not solved in the present paper.

7 Conclusions

The possible violation of isotropy in CMB has been a subject of intense research after the publication of WMAP data. The possible alignment of axes corresponding to several diverse data sets in the direction of the Virgo cluster makes this extremely interesting. Despite several proposals the origin of this effect is so far unknown.

We have developed a general method to test for statistical isotropy in the CMB data. The method assigns three orthogonal eigenvectors and the corresponding eigenvalues for each l multipole. The dispersion in the eigenvalues is quantified by defining the concept of power entropy and provides a measure of the violation of statistical isotropy. The principal eigenvector,

i.e. the eigenvector corresponding to maximum eigenvalue, can also be compared across different multipoles. This yields another measure of violation of isotropy. We also define the concept of alignment entropy which tests for dispersion in the principal eigenvectors across a range of l values. We apply these techniques to the foreground cleaned DA maps provided by the WMAP team for their 3-year and 5-year data.

We find that some of the DA maps, particularly those corresponding to Q band, show signal of significant violation of statistical isotropy. We are unable to attribute this violation to known foreground contamination. Assuming that the signal arises dominantly due to foregrounds, we obtain an estimate of the residual foreground contamination in these maps. We also find a significant signal of anisotropy if we combine the results obtained from all the DAs. The V and W band do not by themselves yield a significant signal of anisotropy. However the violation of isotropy in these DAs is much stronger in the 5 year data in comparison to the 3 year data. This suggests that the signal of anisotropy in these data sets may be masked by the presence of large detector noise and may become much more significant as we accumulate more data.

We do not find a signal of significant alignment with the quadrupole in the present data. In an earlier paper (Samal *et al* 2008) we did find a significant signal in the ILC map in the low multipole range. In this range of multipoles the ILC map is most reliable. This leads us to conclude that alignment with the quadrupole may be present only at low multipoles. The presence of residual foregrounds and detector noise in individual DA maps, however, may hide a signal of alignment. In our studies using alignment entropy we find a highly significant signal of anisotropy for the Q band. This is consistent with the results we found using power entropy. A conservative interpretation is that the Q band anisotropy arises due to residual foregrounds. However we are unable to attribute the alignment in the Q to known foregrounds. The principal axes, for all the multipole ranges considered, are consistent with one another and do not agree well with those found by using simulated data with PSM foreground templates. Our results indicate the existence of some unknown foreground contamination or some other effect.

In the W band we find an improbable level of isotropy in the data. This is quite unexpected. We considered whether there might be due to incorrect assumptions in our random simulations. Yet the assumptions we make are standard. Excess isotropy appears to be a serious problem. This has implications beyond the issues addressed here. It would be interesting to test

the common assumption that detector noise is inherently uncorrelated. The question is important since incorrect modelling of detector noise may also lead to bias in the estimation of CMB power and the cosmological parameters.

8 Acknowledgments

We acknowledge the use of Legacy Archive for Microwave Background Data Analysis. Some of the results of this work are derived using the publicly available HEALPIX package (Górski *et al.*, 2005). Pramoda K. Samal acknowledges CSIR, India for financial support under the research grant CSIR-SRF-9/92(340)/2004-EMR-I. John P. Ralston is supported in part under DOE Grant Number DE-FG02-04ER14308. A portion of the research described in this paper was carried out at the Jet Propulsion Laboratory, California Institute of Technology, under a contract with the National Aeronautics and Space Administration.

References

- Abramo, L. R., Sodre Jr., L., Wuensche, C. A., 2006, Phys. Rev. D74, 083515
- Armendariz-Picon, C., 2004, JCAP 0407, 007
- Armendariz-Picon, C., 2006, JCAP 0603, 002
- Battye, R. A., Moss, A., 2006, Phys. Rev. D74, 04130
- Berera, A., Buniy, R. V., Kephart, T. W., 2004, JCAP 0410, 016
- Bernui, A., 2008, arXiv:0809.0934
- Bernui, A., Villela, T., Wuensche, C. A., Leonardi, R., Ferreira, I., 2006, Astron. Astrophys. 454, 409
- Bernui, A., Mota, B., Reboucas, M. J., Tavakol, R., 2007, Astron. Astrophys. 464, 479
- Bietenholz, M. F., Kronberg, P. P., 1984, ApJ, 287, L1-L2
- Bielewicz, P., Górski, K. M., Banday, A.J., 2004, MNRAS, 355, 1283

Bielewicz, P., Eriksen, H. K., Banday, A. J., Górski, K. M., Lilje, P. B., 2005, ApJ 635, 750

Birch, P., 1982, Nature, 298, 451

Boehmer, C. G., Mota, D. F., 2008, Phys. Lett. B663, 168

Buniy, R. V., Berera, A., Kephart, T. W., 2006, Phys. Rev. D73, 063529

Campanelli, L., Cea, P., Tedesco, L., 2007, arXiv:0706.3802

Cline, J. M., Crotty, P., Lesgourgues, J., 2003, JCAP 0309, 010, astro-ph/0304558;

Contaldi, C. R., Peloso, M., Kofman, L., Linde, A., 2003, JCAP 0307, 002, astro-ph/0303636

Copi, C. J., Huterer, D., Schwarz, D. J., Starkman, G. D., 2006, MNRAS 367, 79

Copi, C. J., Huterer, D., Schwarz, D. J., Starkman, G. D., 2007, Phys. Rev. D75, 023507

de Oliveira-Costa, A., Tegmark, M., Zaldarriaga, M., Hamilton, A., 2004, Phys. Rev. D 69, 063516, astro-ph/0307282

de Oliveira-Costa, A., Tegmark, M., 2006, Phys. Rev. D74, 023005

Dennis, M. R., 2005, J. Phys. A 38, 1653, arXiv:math-ph/0410004

Dimopoulos, K., Lyth, D. H., Rodriguez, Y., 2008, arXiv:0809.1055

Donoghue E. P., Donoghue, J. F., 2005, Phys. Rev. D71, 043002

Donoghue, J. F., Dutta, K. and Ross, A., 2007, arXiv:astro-ph/0703455

Efstathiou, G., 2003, MNRAS 346, L26, astro-ph/0306431

Erickcek, A. L., Kamionkowski, M., Carroll, S. M., 2008, arXiv:0806.0377

Eriksen, H. K. *et al*, 2004, ApJ 605, 14

Eriksen, H. K. *et al*, 2007a, ApJ 656, 641

Eriksen, H. K., Banday, A. J., Górski, K. M., Hansen, F. K., Lilje, P. B., 2007b, ApJ, 660, L81

Freeman, P. E., Genovese, C.R., Miller, C.J., Nichol, R.C., Wasserman, L., 2006, ApJ, 638, 1

Gaztanaga, E., Wagg, J., Multamaki, T., Montana, A., Hughes, D. H., 2003, MNRAS 346, 47, astro-ph/0304178

Gordon, C., Hu, W., Huterer, D., Crawford, T. 2005, Phys. Rev. D72, 103002

Górski, K.M., Hivon, E., Banday, A.J., Wandelt, B.D., Hansen, F.K., Reinecke, M., & Bartelmann, M., 2005, ApJ, 622, 759

Gumrukuoglu, A. E., Contaldi, C. R., Peloso, M., 2006, astro-ph/0608405

Gumrukuoglu, A. E., Contaldi, C. R., Peloso, M., 2007, arXiv:0707.4179

Hajian, A., Souradeep, T., Cornish, N. J., 2004, ApJ 618, L63

Hajian, A., Souradeep, T., 2006, Phys. Rev. D74, 123521

Hansen, F. K., Banday, A. J., Górski, K. M., 2004, MNRAS, 354, 641

Helling, R. C., Schupp, P., Tesileanu T., 2007, Phys. Rev. D74, 063004

Hunt, P., Sarkar, S., 2004, Phys. Rev. D70, 103518

Hinshaw, G. *et al.*, 2003, Astrophys. J., Suppl. Ser. 148, 63

Hinshaw, G. *et al.*, 2007, ApJ Suppl 170, 288

Hivon, E., *et al.*, 2002, ApJ, 567, 2

Hutsemékers, D., 1998 *A & A*, 332, 41

Hutsemékers, D., Lamy, H., 2001, *A & A*, 367, 381

Hutsemékers, D., Payez, A., Cabanac, R., Lamy, H., Sluse, D., Borguet, B., Cudell, J.-R., 2008, arXiv:0809.3088

Inoue, K. T., Silk, J., 2006, ApJ 648, 23

Jain, P., Narain, G., Sarala, S., 2004, *MNRAS*, 347, 394

Jain, P., Panda, S., Sarala, S., 2002, *Phys. Rev. D* 66, 085007

Jain, P., Ralston, J. P., 1999, *Mod. Phys. Lett. A* 14, 417

Jain, P., Sarala, S., 2006, *J. Astrophysics and Astronomy*, 27, 443

Land, K., Magueijo, J., 2005, *Phys. Rev. D* 72, 101302

Land, K., Magueijo, J., 2006, *MNRAS* 367, 1714

Land, K., Magueijo, J., 2007, *MNRAS* 378, 153

Lew, B., 2008, arXiv:0808.2867

Liu, H., Li, T-P, 2008, arXiv:0806.4493

Kahniashvili, T., Lavrelashvili, G., Ratra, B., 2008, arXiv:0807.4239

Kanno, S., Kimura, M., Soda, J., Yokoyama, S., 2008, *JCAP* 0808, 034

Katz, G., Weeks, J., 2004, *Phys. Rev. D* 70, 063527

Kendall, D. G., Young, A. G., 1984, *MNRAS*, 207, 637

Kesden, M. H., Kamionkowski, M., Cooray, A., 2003, *Phys. Rev. Lett.* 91, 221302, astro-ph/0306597

Koivisto, T., Mota, D. F., 2006, *Phys. Rev. D* 73, 083502

Koivisto, T., Mota, D. F., 2007, arXiv:0707.0279

Magueijo, J., Sorkin, R. D., 2007, *MNRAS Lett.* 377, L39

Moffat, J. W., 2005, *JCAP* 0510, 012

Naselsky, P. D., Verkhodanov, O. V., Nielsen, M. T. B., 2007, arXiv:0707.1484

Payez, A., Cudell, J. R., Hutsemékers, D., 2008, arXiv:0805.3946.

Pereira, S., Pitrou, C., Uzan, J.-P., 2007, arXiv:0707.0736

Pullen, A. R., Kamionkowski, M., 2007, *Phys. Rev. D* 76, 103529

- Prunet, S., Uzan, J.-P., Bernardeau, F., Brunier, T., 2005, Phys. Rev. D71, 083508
- Rakic, A., Rasanen, S., Schwarz, D. J., 2006, MNRAS 369, L27
- Ralston, J. P., Jain, P., 2004, Int. J. Mod. Phys., **D13**, 1857
- Rodrigues, D. C., 2008, Phys. Rev. D77, 023534
- Saha, R., Jain, P. and Souradeep, T., 2006, ApJ Lett., 645, L89
- Samal, P. K., Saha, R., Jain, P. and Ralston, J. P., 2008, MNRAS 385, 1718
- Schwarz, D. J., Starkman, G. D., Huterer, D., Copi, C. J., 2004, Phys. Rev. Lett. 93, 221301
- Slosar, A., Seljak, U., 2004, Phys. Rev. D70, 083002
- Tegmark, M., de Oliveira-Costa, A. and Hamilton, A., 2003, Phys. Rev. D 68, 123523
- Vale, C., 2005, astro-ph/0509039
- Weeks, J. R., 2004, astro-ph/0412231
- Wiaux, Y., Vielva, P., Martinez-Gonzalez, E., Vanderghenst, P., 2006, Phys. Rev. Lett. 96, 151303
- Yokoyama, S., Soda, J., 2008, JCAP 0808, 005

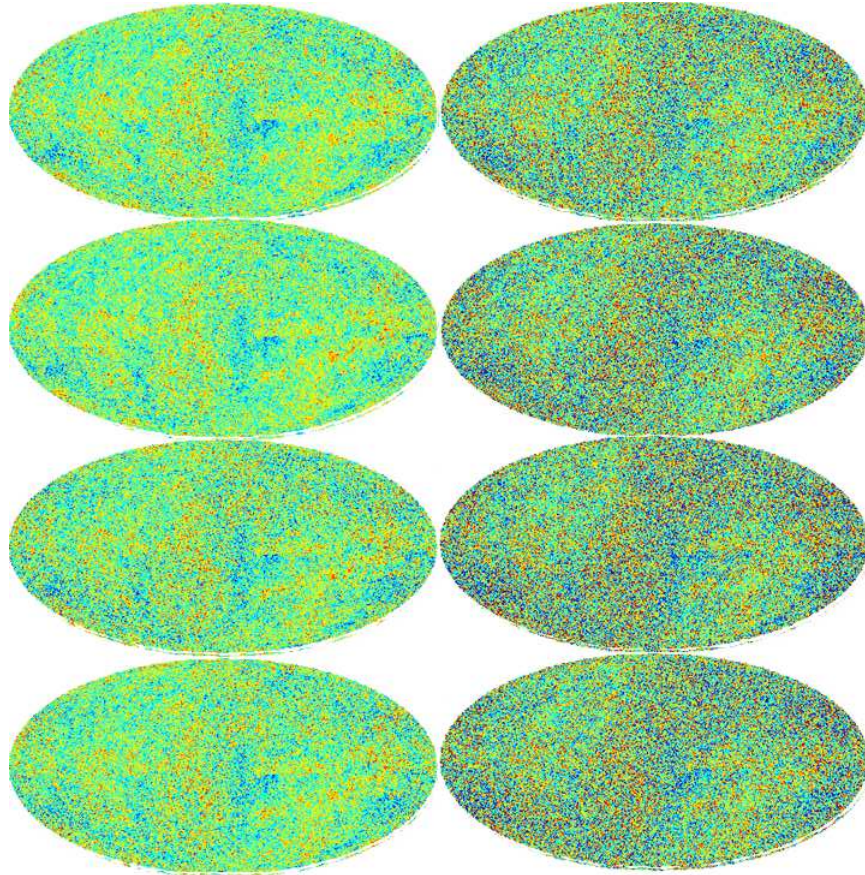


Figure 1: The 3-year maps after filling the $Kp2$ region with randomly generated *CMB* signal and detector noise appropriate for each band. From top to bottom the left panel shows $Q1$, $Q2$, $V1$ and $V2$ DA maps respectively while the right panel shows $W1$, $W2$, $W3$ and $W4$ DA maps.

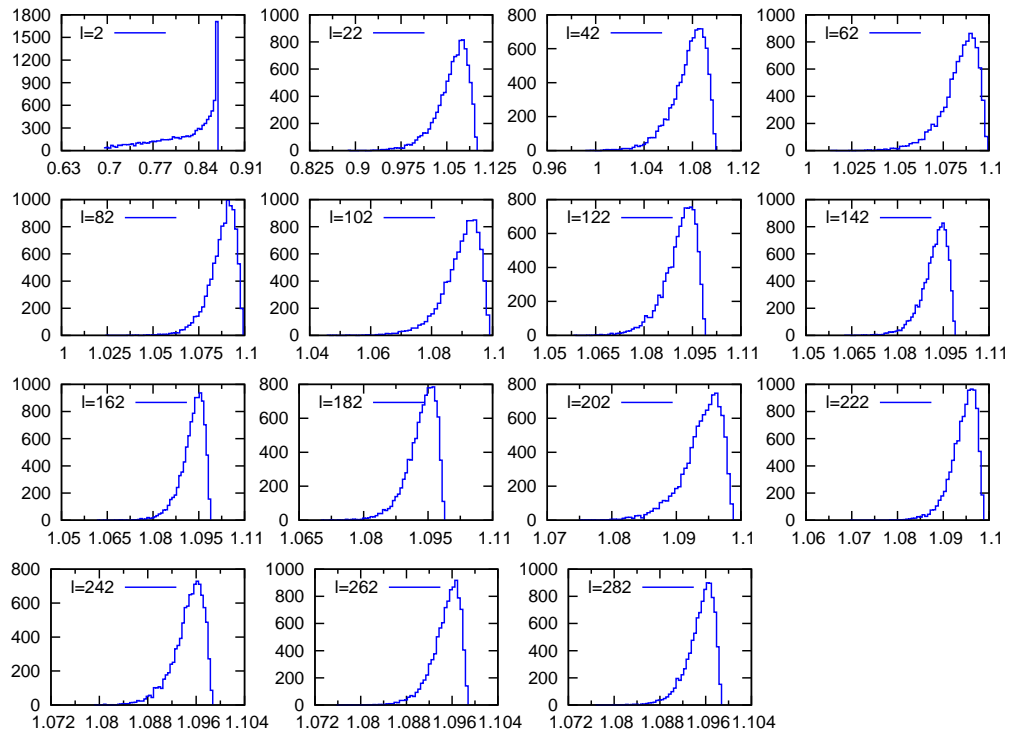


Figure 2: Histograms of the power entropy S_P for multipole range $2 \leq l \leq 300$ at intervals of 20 units using the WMAP 3-year data for the Q_1 map.

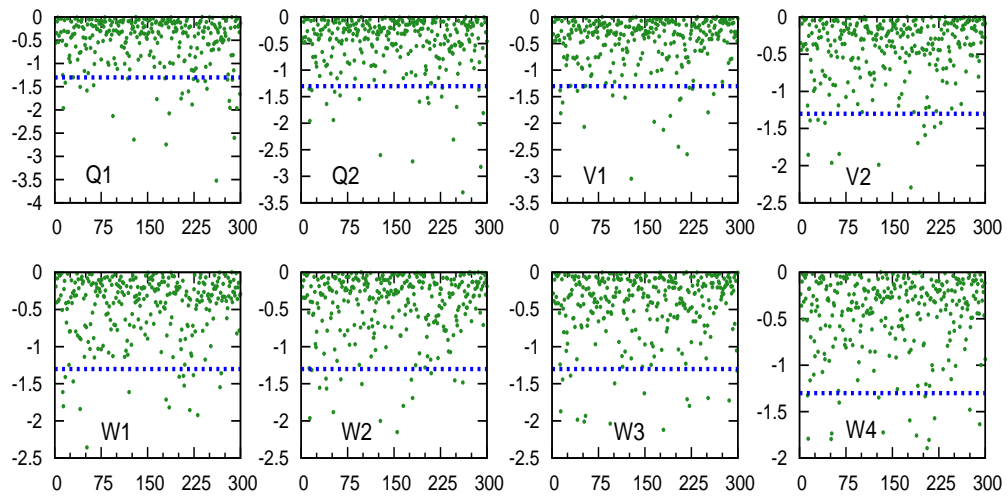


Figure 3: $\log_{10}(P)$ -values of the power entropy from the eight WMAP bands for the range $2 \leq l \leq 300$ for the WMAP 3-year data. The dashed horizontal line shows $P = 0.05$.

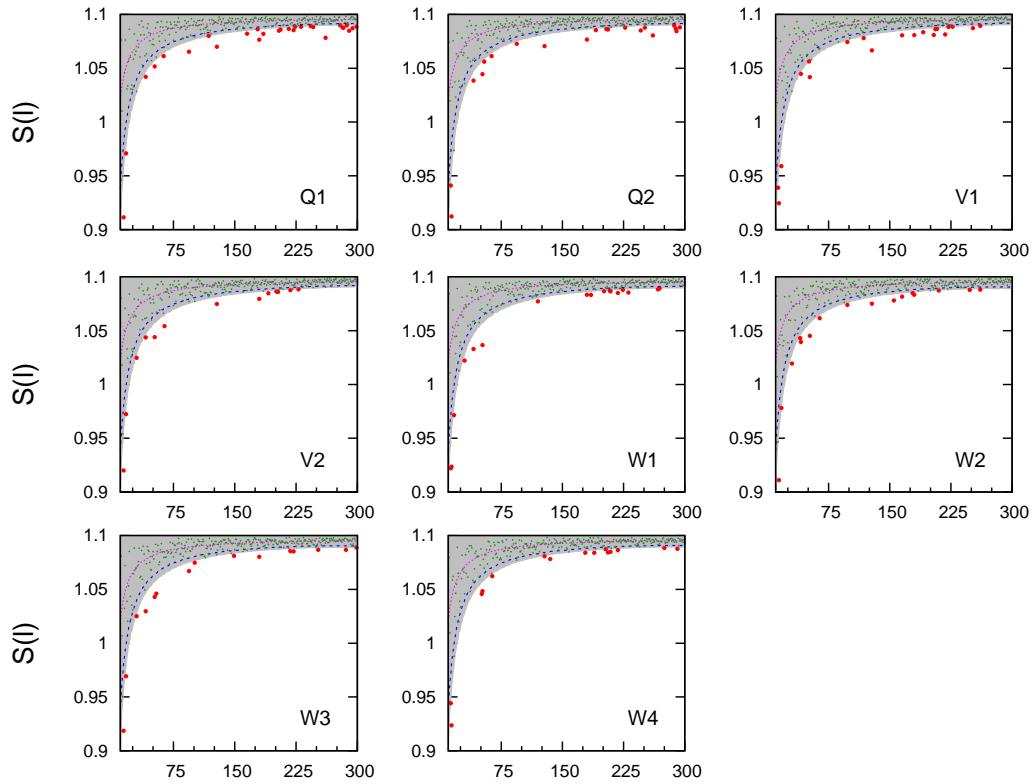


Figure 4: Distribution of the power entropy $S(l)$ showing the 95% confidence level (grey band) for the WMAP 3-year data. Red points show multipoles potentially inconsistent with the isotropic prediction.

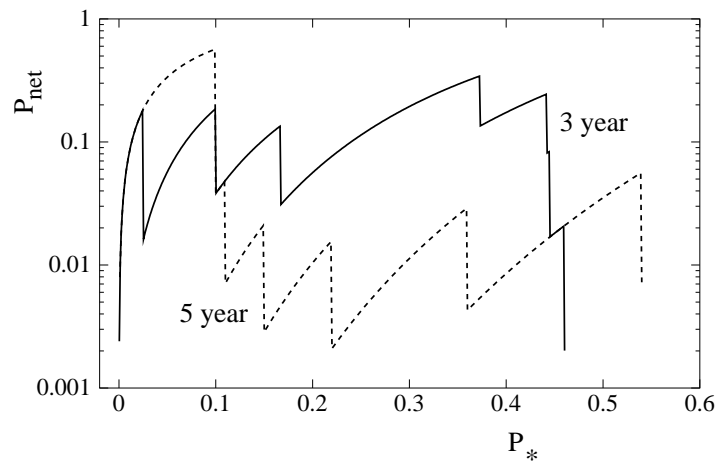


Figure 5: The net probability P_{net} over all the bands selecting power-entropy $P_{\text{band}} < P_*$ for the three (solid line) and five (dashed line) year WMAP data.

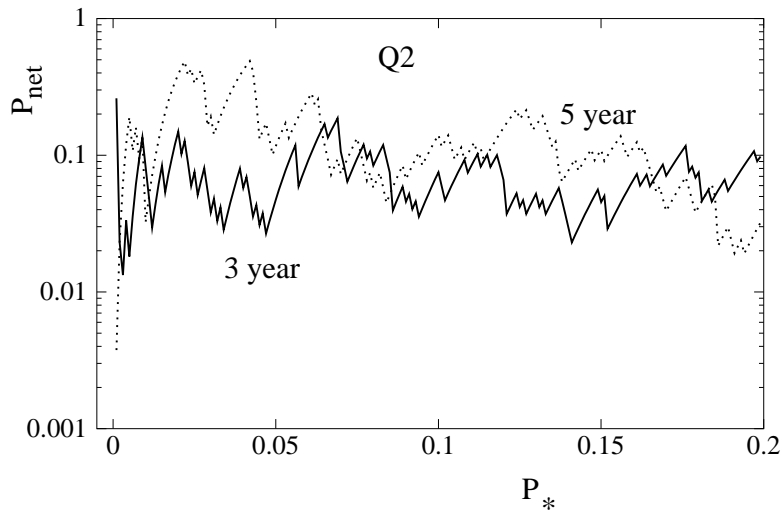
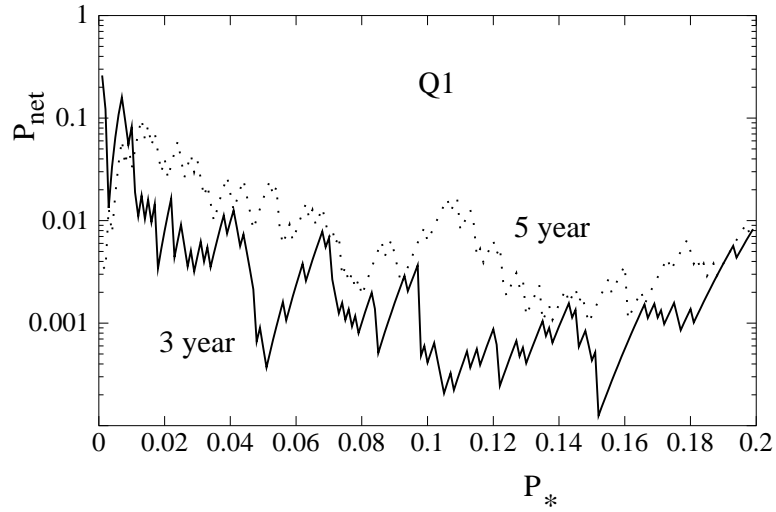


Figure 6: The net cumulative probability P_{net} the DAs $Q1$ and $Q2$ selecting power-entropy $P_{\text{band}} < P_*$ for the three (solid line) and five (dotted line) year WMAP data.

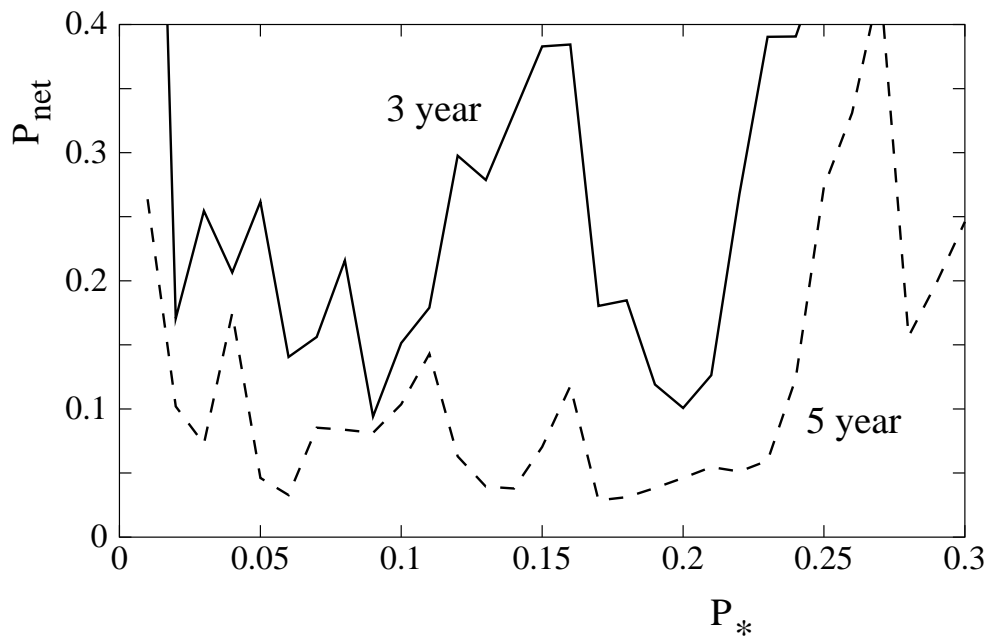


Figure 7: The net cumulative probability P_{net} the DAs $V1$, $V2$, $W1$, $W2$, $W3$ and $W4$ selecting power-entropy $P_{\text{band}} < P_*$ for the three (solid line) and five (dotted line) year WMAP data.

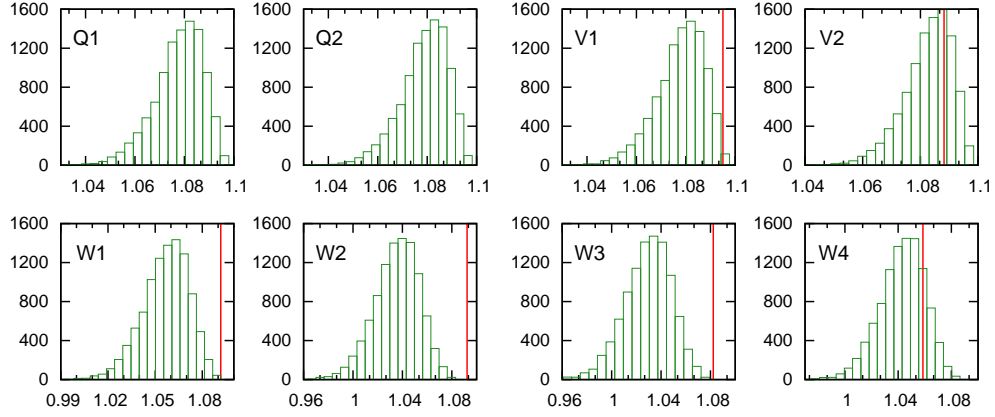


Figure 8: The distribution of the alignment entropy for the statistically isotropic *CMB* plus appropriate detector noise maps for the range $150 \leq l \leq 300$ for the WMAP 3-year data. The alignment entropy measures for different maps are also shown.

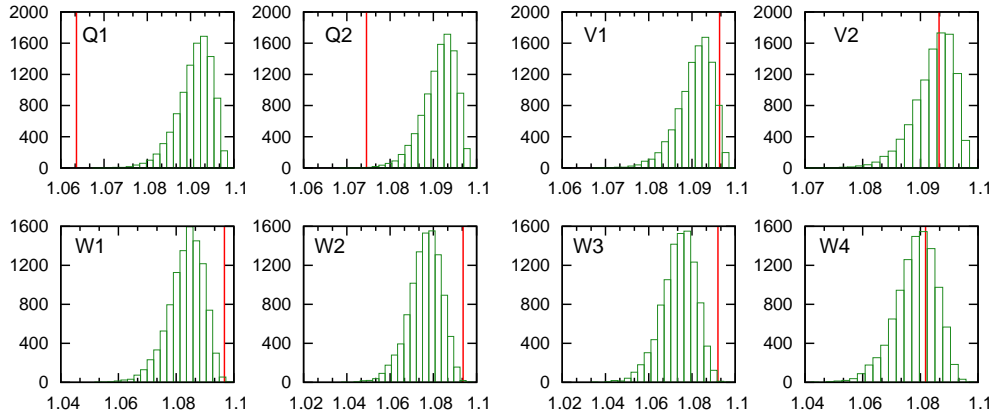


Figure 9: The distribution of the alignment entropy for the statistically isotropic *CMB* plus appropriate detector noise maps for the range $2 \leq l \leq 300$ for the WMAP 3-year data. The alignment entropy measures for different maps are also shown .

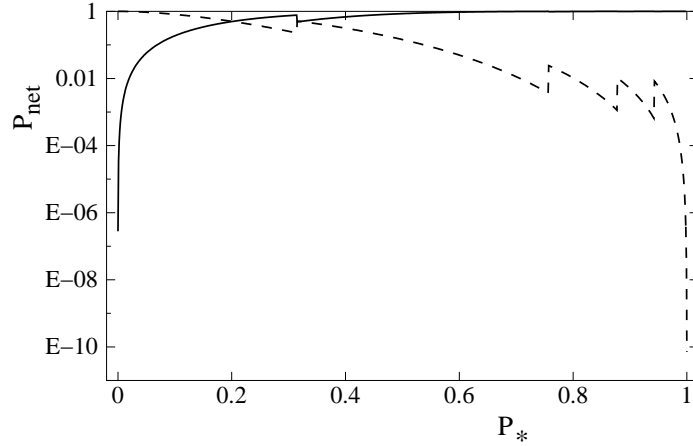


Figure 10: The net probability P_{net} across bands to find excessive anisotropy (solid line) and isotropy (dashed line) with the alignment entropy for the WMAP five year data. Multipole range $150 \leq l \leq 300$.

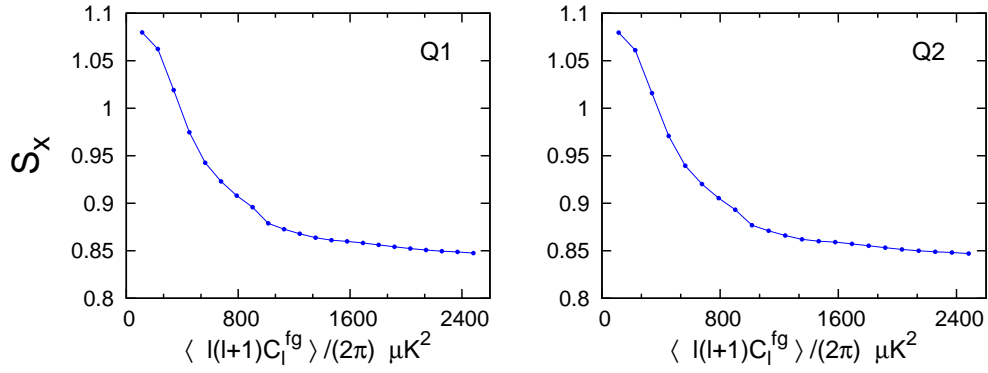


Figure 11: The alignment entropy, S_X , for the bands Q1 and Q2 for the multipole range $150 \leq l \leq 300$ as a function of the average foreground power (see text).

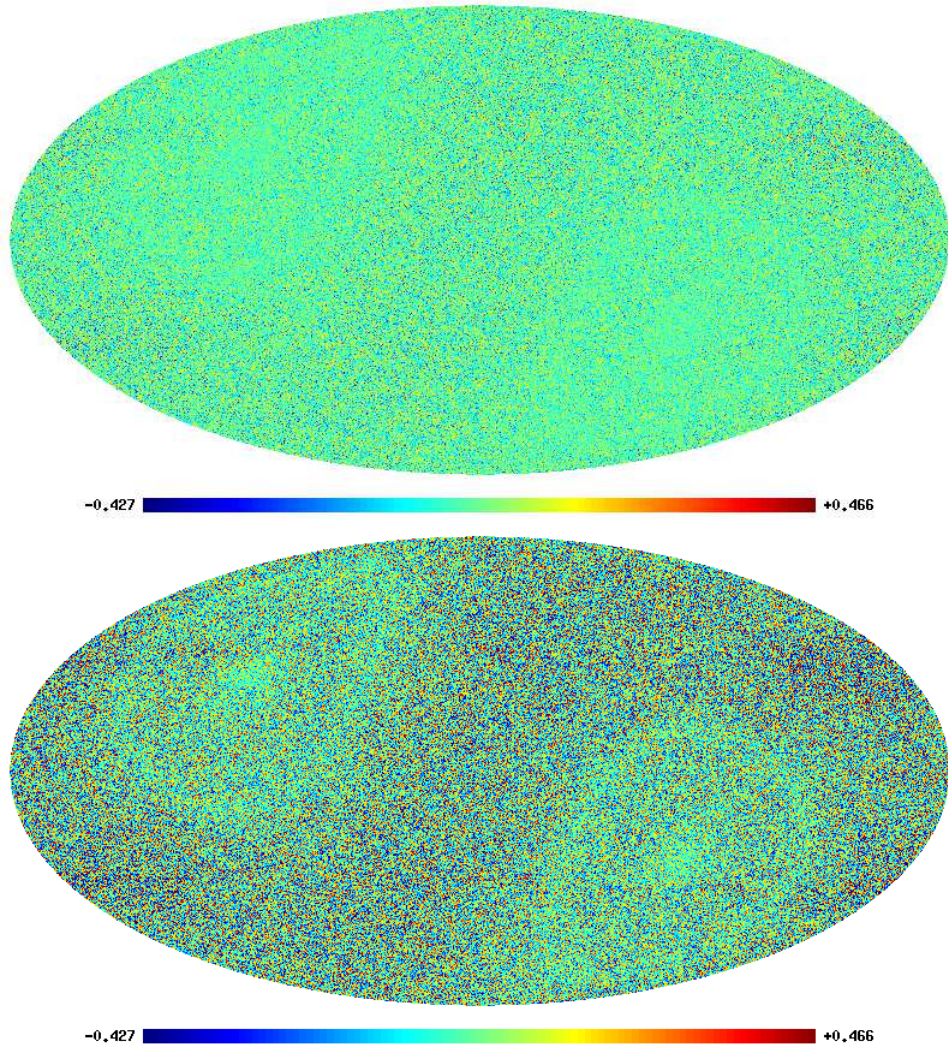


Figure 12: The generated noise maps for $Q1$ (upper) and $W4$ (lower) bands.